In situ trap properties in CCDs: the donor level of the silicon divacancy

Preprint typeset in JINST style - HYPER VERSION

In situ trap properties in CCDs: The donor level of the silicon divacancy

David J. Hall[a]*, Daniel Wood[a], Neil J. Murray[a]†, Jason P. D. Gow[a], Alexander Chroneos[bc] and Andrew Holland[a]

[a] *Centre for Electronic Imaging, The Open University, Walton Hall, Milton Keynes MK7 6AA, UK*
[b] *Faculty of Engineering, Environment and Computing, Coventry University, Priory Street, Coventry CV1 5FB, United Kingdom*
[3] *Department of Materials, Imperial College London, South Kensington Campus, London SW7 2AZ, United Kingdom*

E-mail: david.hall@open.ac.uk

ABSTRACT:
The silicon divacancy is one of the main defects of concern in radiation damage studies of Charge-Coupled Devices (CCDs) and, being immobile at room temperature, the defect is accessible to a variety of characterisation techniques. As such, there is a large amount of (often conflicting) information in the literature regarding this defect. Here we study the donor level of the divacancy, one of three energy levels which lie between the silicon valence and conduction bands. The donor level of the divacancy acts as a trap for holes in silicon and therefore can be studied through the use of a p-channel CCD.

The method of trap-pumping, linked closely to the process of pocket-pumping, has been demonstrated in the literature over the last two years to allow for in-situ analysis of defects in the silicon of CCDs. However, most work so far has been a demonstartion of the techinique. We begin here to use the technique for detailed studies of a specific defect centre in silicon, the donor level of the divacancy. The trap density post-irradiation can be found, and each instance of the trap identified independently of all others. Through the study of the trap response at different clocking frequencies one can measure directly the defect emission time constant, and through tracking this at different temperatures, it is possible to use Shockley-Read-Hall theory to calculate the trap energy level and cross-section.

A large population of traps, all with parameters consistent with the donor level of the divacancy, has been studied, leading to a measure of the distribution of properties. The emission time constant, energy level and cross-section are found to have relatively large spreads, significantly beyond the small uncertainty in the measurement technique. This spread has major implications on the correction of charge transfer inefficiency effects in space applications in which high precision is required.

KEYWORDS: Divacancy, CCD, defect, trap, pocket-pumping, trap-pumping, radiation damage, p-channel.

Contents

1. Introduction

The Charge-Coupled Device (CCD) has been one of the main detectors of choice for space science and astronomy missions for several decades. When used in space, the detectors are subjected to an often harsh radiation environment. This radiation, dominated by high energy particles such as protons and electrons and dependent on the location and orbit, can cause significant damage to devices. As the science goals of missions such as Euclid [1] and Gaia [2] become evermore demanding, the impact of radiation on the detector performance becomes increasingly important. Without sufficient mitigation and correction, radiation damage effects could destroy the chances of a mission achieving its full science goals for a significant portion of the mission lifetime.

When a high-energy proton passes through the silicon of a CCD, silicon atoms can be displaced from their lattice positions, creating vacancies (absences of silicon atoms at lattice positions) that are highly mobile and can diffuse through the lattice until they form a stable defect state at the current temperature. The stable state may be formed by a vacancy coupling to an impurity or dopant atom, such as in the Si-A centre (vacancy with oxygen [3]) or Si-E centre (vacancy with phosphorous [4]), or with another vacancy to form the divacancy (Section 2). The defect structures produced can create additional energy levels between the valance and conduction bands in the silicon.

The mid-gap energy levels act as trapping centres for charge carriers as they are transferred through the device, with charge carriers being captured and then released at a later time (determined by the trap emission time constant), smearing the resulting image. In an n-channel CCD, the signal is generated and stored as electrons, and therefore the energy levels near the conduction band (acceptor levels) can act as electron traps. In a p-channel CCD, the signal is generated and stored

*Corresponding author.

†Now at Dynamic Imaging Analytics Limited, Bletchley Park Science and Innovation Centre, MK3 6EB

as holes, and therefore the energy levels near the valance band (donor levels) can act as hole traps. The issue of the 'radiation hardness' of a detector, be that n-channel or p-channel, has often been compared [5], but what is most relevant here is the difference in the densities of the trap species that are most detrimental to the achievement of the mission science goals. If one wishes to measure the number of photons detected, the smearing of signal by one or two pixels may not have a major impact and the total signal can be summed. However, if one wishes to measure shape changes to objects being detected, then a small shift of the signal by one or two pixels is the most detrimental to the science performance. For this reason, one must know the full details of the trap species present and in what densities they are produced for any specified radiation dose.

Each trap species will have a related emission time consant, dependent on the distance between the energy level and the valance or conduction band, that defines the release of trapped holes or electrons respectively. The probabilities of capture and emission of charge can be calculated using Shockley-Read-Hall theory [6] [7]. It is these probabilities that can be used to probe the parameters of individual traps within a CCD through the technique of trap-pumping. This technique has been demonstrated over the last two years as a very effective method of investigating trap properties, although results published so far are limited to conference proceedings and proof of concept demonstrations, such as in [8] and [9]. Here we present a more in depth study of the donor level of a single defect species, the divacancy, in a p-channel CCD.

2. The Divacancy

In a radiation environment a divacancy can be formed by the agglomeration of two vacancies (vacancies are mobile even at low temperatures) or the simultaneous displacement of two adjacent silicon atoms from their lattice sites, Figure 1(a). From a technological viewpoint, the divacancy is considered to be the most important intrinsic defect in silicon and it is stable even at room temperature [10]. The two missing atoms, shown in grey on Figure 1(a), affect the bonding of the lattice thus causing an "extended bond" to form, as shown by the dotted line; it is in this region that the electrons or holes are thought to be "captured" by the related acceptor or donor levels respectively.

From an experimental viewpoint the divacancy has four charge states (+1, 0, -1, -2) [11] introducing in the band gap three deep energy levels [12]. These trap levels correspond to a singly ionised donor state (0/+), a singly ionised acceptor state (–/0) and doubly ionised acceptor state (=/–). The donor level will act to trap holes within a p-channel CCD, whilst the two acceptor levels will trap electrons in an n-channel CCD. In both detector flavours the emission time constants associated with each trap energy level fall within the timescales that have a noticeable and detrimental impact on device readout for typical readout and operating temperatures.

In a review by Pichler [14] it is concluded that Deep Level Transient Spectroscopy (DLTS) measurements generally agree on the single and double acceptor levels being found at $E_c - 0.39$ to 0.43 eV and $E_c - 0.21$ to 0.23 eV respectively (refer to Table 2.9 in [14]). In the same review, the donor level of the divacancy was found to be reported between $E_v + 0.18$ and 0.23 eV, although more recent studies confirm the donor level being situated around $E_v + 0.19$e eV. The energy levels of the three states are shown diagrammatically in Figure 1(b).

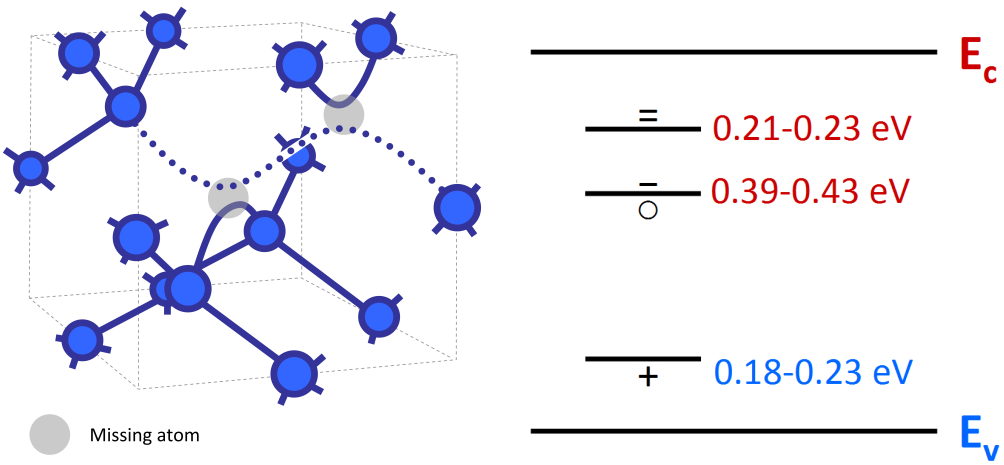

(a) A diagrammatic interpretation of the divacancy showing the two 'missing' silicon atoms or vacancies, based on a representation from [13].

(b) Three energy levels between the valence and conduction band in silicon are associated with the divacancy. Energy levels are taken from [14].

Figure 1. The divacancy in silicon.

In a more recent study, Mostek *et al.* [15], using a variant of pocket-pumping, albeit in the temperature domain rather than in the time domain as discussed in Section 3, suggests that the donor level of the divancy is situated at $E_v + 0.184 \pm 0.012$ eV. This result, consistent with the results discussed above, was chosen as the starting point for our study. Here, however, we use a more powerful variation of the pocket pumping technique, as discussed in the following section, in which we are able to analyse the properties of individual defects in great detail.

3. Single-trap Pumping Technique

Whilst there are many techniques that allow the study of defects (traps) in the silicon lattice (e.g. Deep Level Transient Spectroscopy (DLTS) [16]), the majority of these techniques only allow the study of full populations of traps in a device. Averaged properties of trap species can be calculated but there is no way to study the distribution of individual trap properties across a device.

Pocket pumping [17] can be used to study potential pockets in a device. The device is exposed to a flat-field of signal before the charge generated is "pumped" back and forth between two or more row pixels or register elements. As the charge packets pass over potential pockets in the device, charge is captured and later emitted, building up signal "dipoles" in the image, i.e. one dark pixel (from which charge has been removed) and a neighbouring bright pixel (into which charge has been deposited), Figure 2(a). The amplitudes of the bright and dark pixels are equal and opposite and are dependent on the properties of the pocket (or trap) and how these relate to the conditions of operation.

More recently, pocket pumping has been developed to allow the location and trapping efficiency of single traps to be found [18]. Through the careful selection of the operating conditions it has been demonstrated that the properties of individual defects or traps in the silicon of a CCD

can not only be located, but the emission time constant of each individual trap can be found within uncertainties of only a few percent [19]. Using this powerful technique it is now possible to study the properties of traps in the CCD, with locations known at the sub-pixel level, and to see the actual distribution of the energy levels and capture cross-sections of traps.

This single-trap pumping technique is explained in detail in [19]; only a brief summary is provided here for ease of reference, considering a three-phase device for demonstration purposes. A four-phase device can equally be studied through the clocking of one pair of neighbouring phases as a single "phase".

Following illumination with a flat-field of signal under, for example, Phase 1, the charge in the device is shuffled to Phase 2, then Phase 3, into Phase 1 in the neighbouring pixel and then back through phases 3 and 2 until the charge returns to its initial position, Figure 2(b). For the example shown of a trap being present under Phase 2, an electron is only transferred from one charge packet to its nearest neighbour if it is emitted between one clock period after capture ($> t_{ph}$) and before two clock periods have passed ($< 2t_{ph}$). Using Shockley-Read-Hall theory [6][7], the probability of an electron being transferred during one clocking cycle is found [19] to be given by Equation 3.1.

$$P_p = \exp\left(\frac{-t_{ph}}{\tau_e}\right) - exp\left(\frac{-2t_{ph}}{\tau_e}\right) \tag{3.1}$$

Repeating the cycle a number of times, N, and assuming a probability of capture for the trap in question of P_c, to a first approximation the amplitude I of the dipole is described by Equation 3.2. By repeating the pumping at a range of clock periods a profile for each dipole can be produced to which the fitting of Equation 3.2 will allow the determination of the trap emission time constant and capture probability. Furthermore, if the process is repeated over a range of temperatures, through the use of Shockley-Read-Hall theory one can find the energy level and cross-section of each individual trap within the CCD independently of all others[1].

$$I = NP_c\left(\exp\left(\frac{-t_{ph}}{\tau_e}\right) - exp\left(\frac{-2t_{ph}}{\tau_e}\right)\right) \tag{3.2}$$

From a starting position of Phase 1, only traps in phases 2 and 3 show dipoles, with the phase of the dipole determined by the polarity. To find traps in Phase 1, the pumping cycle must begin in either Phase 2 or Phase 3.

4. Experimental Study

To study the donor level of traps in-situ, one must use a p-channel CCD; we are looking here into the trapping and emission of holes rather than electrons. For this purpose, an e2v p-channel CCD, made using the same mask-set as the e2v CCD204, was irradiated at the Kernfysisch Versneller Instituut (KVI) to a fluence of 2×10^9 protons per cm^2 (10 MeV equivalent) at a primary beam energy of 190 MeV that was reduced to 50 MeV before the device. The p-channel CCD204-22 has a four-phase image area of 4k $\times$ 1k $\times$ 12 µm pixels. An area in the device of 1000 $\times$ 888 pixels in one half was selected in the irradiated region (at the limits of the flatness of the irradiation) and

[1] To identify individual traps it is required that the trap density is low enough such that the traps to be analysed are seperated from neighbouring traps by one pixel or more.

compared with a non-irradiated area (shielded during the irradation) of 501 × 888 pixels; these regions were selected as the maximum areas available for analysis, limited by the edges of the masking used for the irradiation of the device.

Using the method detailed above (Section 3) and explained in more detail in [19], the image-area of the device was clocked for values of t_{ph} (the dwell time under each phase) ranging from 2 µs to 20 ms, with the step-length varying from approximately 2 µs to 150 µs to efficiently cover the time range. At least 100 images (and therefore 100 different values of t_{ph}) were taken at each temperature studied.

Three temperatures were selected to allow the determination of the energy level and cross-section of the traps encountered: -114.0±0.1°C, -119.2±0.1°C and -124.0±0.1°C. The temperatures were selected to allow coverage of the expected emission time constant range for the donor level of the divacancy from the literature (see Section 2).

Phases 1 and 2 were clocked together to create a pseudo-three-phase pumping scheme (i.e. 1&2, 3, 4, 1&2, 4, 3, restart) 4000 times (from Equation 3.2, $N = 4000$). A flat-field of approximately 25000 holes signal was provided by a Light-Emitting Diode (LED) in the vacuum chamber, providing the background signal to be "pumped".

Dipoles with an amplitude greater than 3σ above the local background signal were automatically found in the images and the amplitudes I then tracked through all images across all values of t_{ph}. The data produced (i.e. I vs. t_{ph}) were then fitted independently with Equation 3.2 to provide the emission time constant τ_e and capture probability.

The analysis presented below is restricted to dipoles which had what was deemed a 'good fit' to the analytical function (Equation 3.2). The function was fitted to the data using a non-linear minimisation of the sum of squared residuals. The strength of the fit is parameterised by a Pearson's correlation coefficient r with a magnitude between positive one and zero, one being a perfect fit to the data, zero being no correlation [20]. The cut-off was taken at $r = 0.9$ to provide a balance between the number of dipoles analysed and the standard deviation of the resulting emission time constants; as the r value cut-off decreases, although the number of dipoles selected for analysis increases, the standard deviation of the emission time constant distribution also increases, implying the unwanted inclusion of non-divacancy-like defects in the analysis.

5. Results

The number of dipoles identified provides an estimate of the number of divacancy defects present in both the irradiated and control sections of the device. For the control section the defect density has been found to be $(3.1 \pm 0.4) \times 10^{-3}$ pixel^{-1}. Following an unbiased irradiation at room temperature, the irradiated region of device provided a defect density of $(1.1 \pm 0.1) \times 10^{-1}$ pixel^{-1}. In both cases, from the associated emission time constants, the defects are consistent with the donor level of the divacancy.

The values given are averaged across all three temperatures tested and have been corrected to reflect that the trap-pumping technique only probes defects beneath certain regions of the barrier-phase electrodes; the volumes probed were analysed using the model detailed in Skottfelt *et al.* [21]. It is important to note that these values do not reflect the true number of divacancies present in the entire pixel volume, but rather the number that can be assumed to interact with a signal

charge cloud of this size. This charge cloud size can be cross-referenced with the charge packet density using Silvaco Atlas simulations [21].

For each identifiable dipole an intensity curve was produced at each phase time tested and subsequently fitted with a curve corresponding to Equation 3.2. Fitting was carried out using the Nelder-Mead method which gives an unconstrained, non-linear minimization of the sum of squared residuals. The strength of the fit was defined by the Pearson correlation coefficient, using a minimum threshold of 0.90.

Once intensity curves have been fitted the defect emission time constants are obtained from the related fit parameters. For those defects producing reliable curves at all three temperatures, the emission time constant was plotted against temperature, as shown in Figure 3(a). Each line in the figure corresponds to a single tracked defect across three temperatures.

In Figure 4 we show the distribution of the divacancy emission time constants at the three temperatures tested. The distribution contains a relatively large spread, albeit smaller than the total spread suggested in [15]. The measurement uncertainty for this method has been calculated from the deviation of the individual defect curves (Figure 3(a)) from a SRH-based characterstic curve and has been found to be of the order of a few percent; this value varies slightly from trap-to-trap depending on their location within the charge packet (and therefore probability of capture and dipole intensity). Therefore, it is believed this is a *genuine spread*, possibly related to minor variations in the defect structure (e.g. the exact alignment of the silicon atoms and that of the surrounding lattice).

The curves shown in Figure 3(a) can be fit based on SRH theory to determine the energy level and cross-section of the responsible defect. The distribution of calculated energy levels and cross-sections are shown in Figure 5 and Figure 6 respectively.

The mean energy level above the valence band edge is found to be 0.20 ± 0.02 ($\pm$ 0.005) eV, where the value of 0.02 eV represents a genuine spread which is seen in the calculated energy levels but does not arise from measurement uncertainty (measured at 0.005 eV). Although we see a range of energies, the grouping of energy levels shows no discernible trends that would be consistent with a variation in trap species; we believe all the traps that have been analysed and presented here to be the divacancy.

The mean value for the cross-section has been found to be 3×10^{-15} cm^2. It is worth noting that uncertainties in the normal sense are not relevant here as we expect genuine spread in cross-section values due to field, temperature dependencies and other effects which are contained within the capture cross-section. We see a range in the cross-section of 7×10^{-16} cm^2 to 9×10^{-15} cm^2 for approximately one sigma above and below the mean.

It might be expected that the defects with the longest emission time constants (i.e. the 'slowest' defects) are those which lie furthest from the band edge. Figure 7 shows the relationship between the emission time constant of each defect and the calculated values of energy for each defect analysed. It can be seen in Figure 7 that although there is a possible broad trend between longer emission time constants and higher calculated energy levels, the distribution is otherwise fairly evenly spread. This leads us to believe that a number of factors are responsible for the large spread in the emission time constant distribution, as indicated above, rather than a single cause.

Table 1. Summary of the results found for the divacancy through the experiemental study detailed in Section 5

Irradiation fluence	2×10^{9} protons cm^{2} (10 MeV equivalent)
Divacancy density	$(1.1 \pm 0.1)\times10^{-1}$ pixel^{-1}
Trap energy	0.20 ± 0.02 ($\pm$ 0.005) eV
cross-section	3×10^{-15} cm^{2} (7×10^{-16} cm^{2} to 9×10^{-15} cm^{2})

6. Conclusions

The divacancy can be a particularly troublesome defect in both n-channel and p-channel CCDs, with an emission time constant within the desirable range of clock timings. The donor-level of the divacancy, capable of capturing holes, is of particular importance for the study of p-channel CCDs as a possible future replacement for n-channel CCDs in space astronomy telescopes. Through the use of the trap-pumping technique, over 40,000 single occurances of the divacancy have been studied individually. The collective properties of the studied population of divacancies are summarised in Table 1.

Perhaps of most signficance is the measure of the distribution of the properties of the popultion of traps that are all considered to be within the scope of the properties expected of the divacancy. This relatively large spread in emission time constants measured, and consequently in the calculated energy levels and cross-sections, suggests that we are measuring the impact of, for example, small deviations in the silicon lattice surrounding the defect locations.

A similar analysis is possible on other trap species for both n-channel and p-channel CCDs. Through the use of the methods detailed in this paper, a deeper understanding and more detailed analysis of the parameters of the dominant trap species in CCDs can be implemented, leading to improved device operating modes to minimise the impact of the traps [22]. As science goals become more demanding, the understanding of defects in CCDs for space applications becomes ever more important to mission success. The fine line between the success and failure of a mission may depend on the ability to mitigate and correct radiation damage effects. With the increased knowledge gained throught trap-pumping, studying individual traps in-situ, we will be able to make great strides forwards towards more substantial mitigation and more accurate correction of images from radiation-damaged CCDs.

Acknowledgments

With thanks to e2v technologies for their continued support in this research and to the European Space Agency (ESA) for providing the devices for testing. The results from this study are taken from experimental testing run alongside a larger, ongoing, ESA-funded study into radiation damage in p-channel CCDs.

References

[1] R. Laureijs, *et al.* (2011, Oct). Euclid Definition Study Report, ArXiv e-prints 1110.3193 [Online]. Available: http://arxiv.org/abs/1110.3193.

[2] L. Lindegren *et al.*, *The Gaia mission: science, organization and present status*, *Proc. International Astronomical Union*, **248** (2008) 217.

[3] A. Chroneos *et al.*, *Oxygen defect processes in silicon and silicon germanium*, *Applied Physics Reviews*, **2** (2015) 021306.

[4] H. Wang *et al.*, *Phosphorous-vacancy-oxygen defects in silicon*, *Journal of Materials Chemistry A* **1(37)** (2013) 11384âĂŞ11388.

[5] J. Gow *et al.*, *Proton damage comparison of an e2v technologies n-channel and p-channel CCD204*, *IEEE Transactions on Nuclear Science*, **61(4)** (2014) 1843-1848.

[6] W. Shockley and W. T. Read Jr., *Statistics of the recombinations of holes and electrons*, *Phys. Rev.*, **87(5)** (1952) 835-842.

[7] R. N. Hall, *Electron-hole recombination in germanium*, *Phys. Rev.*, **87(5)** (1952) 387-387.

[8] D. J. Hall *et al.*, *Studying defects in the silicon lattice using CCDs*, *Journal of Instrumentation*, **9(12)**, (2014) C12004.

[9] D. Wood *et al.*, *Studying charge-trapping defects within the silicon lattice of a p-channel CCD using a single-trap "pumping" technique*, *Journal of Instrumentation*, **9(12)**, (2014) C12028.

[10] S. R. G. Christopoulos *et al.*, *VV and VO2 defects in silicon studied with hybrid density functional theory*, *J. Mater. Sci. Mater. Electron*, **26** (2015) 1568-1571.

[11] Y. H. Lee and J. W. Corbett, *EPR studies of defects in electron-irradiated silicon: A triplet state of vacancy-oxygen complexes*, *Phys. Rev. B*, **13** (1976) 2653.

[12] B. G. Svensson *et al.*, *Divacancy acceptor levels in ion-irradiated silicon*, *Phys. Rev. B*, **43** (1991) 2292.

[13] J. W. Corbett and G. D. Watkins, *Silicon Divacancy and its Direct Production by Electron Irradiation*, *Phys. Rev. Lett.*, **7(8)** (1961) 314.

[14] P. Pichler, *Intrinsic Point Defects, Impurities, and Their Diffusion in Silicon*, Computational Microelectronics, Springer (2004).

[15] N. J. Mostek *et al.*, *Charge trap identification for proton-irradiated p+ channel CCDs*, *Proc. SPIE*, **7742** (2010) 774216.

[16] D. V. Lang, *DeepâĂŘlevel transient spectroscopy: A new method to characterize traps in semiconductors*, *J. Appl. Phys.*, **45** (1974) 3023.

[17] J. R. Janesick, *Scientific charge-coupled devices*, SPIE Press (2001).

[18] N. J. Murray *et al.*, *Mitigating radiation-induced charge transfer inefficiency in full-frame CCD applications by 'pumping' traps*, *Proc. SPIE*, **8453** (2012) 845317.

[19] D. Hall *et al.*, *Determination of In Situ Trap Properties in CCDs Using a "Single-trap-pumping" Technique"*, *IEEE Transactions on Nuclear Science* **61(4)** (2014) 1826-1833.

[20] K. Pearson, *Notes on regression and inheritance in the case of two parents*, *Proceedings of the Royal Society of London*, **58** (1985) 240âĂŞ242.

[21] J. Skottfelt *et al.*, *Comparing simulations and test data of a radiation damaged CCD for the Euclid mission*, *Proc. SPIE*, **9915**, (2016) 991529.

[22] D. Hall *et al.*, *Optimisation of device clocking schemes to minimise the effects of radiation damage in charge-coupled devices*, *IEEE Transactions on Electron Devices*, **59(4)** (2012) 1099-1106.

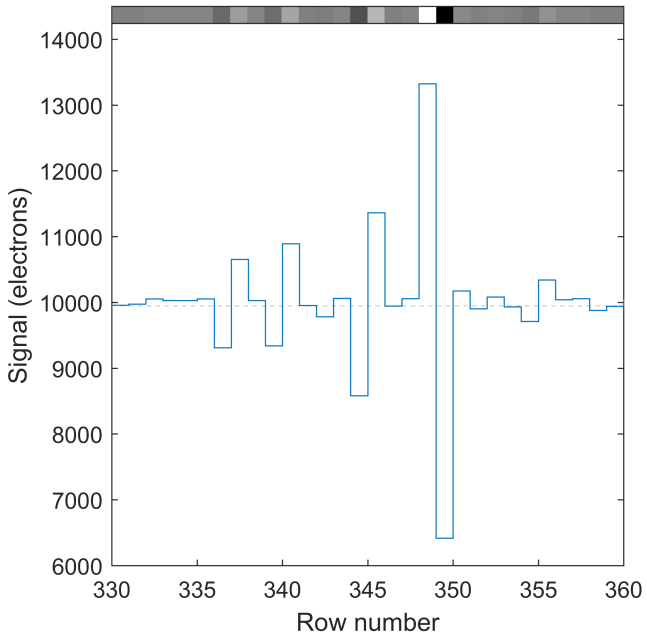

(a) Single row of pumped signal showing five dipoles.

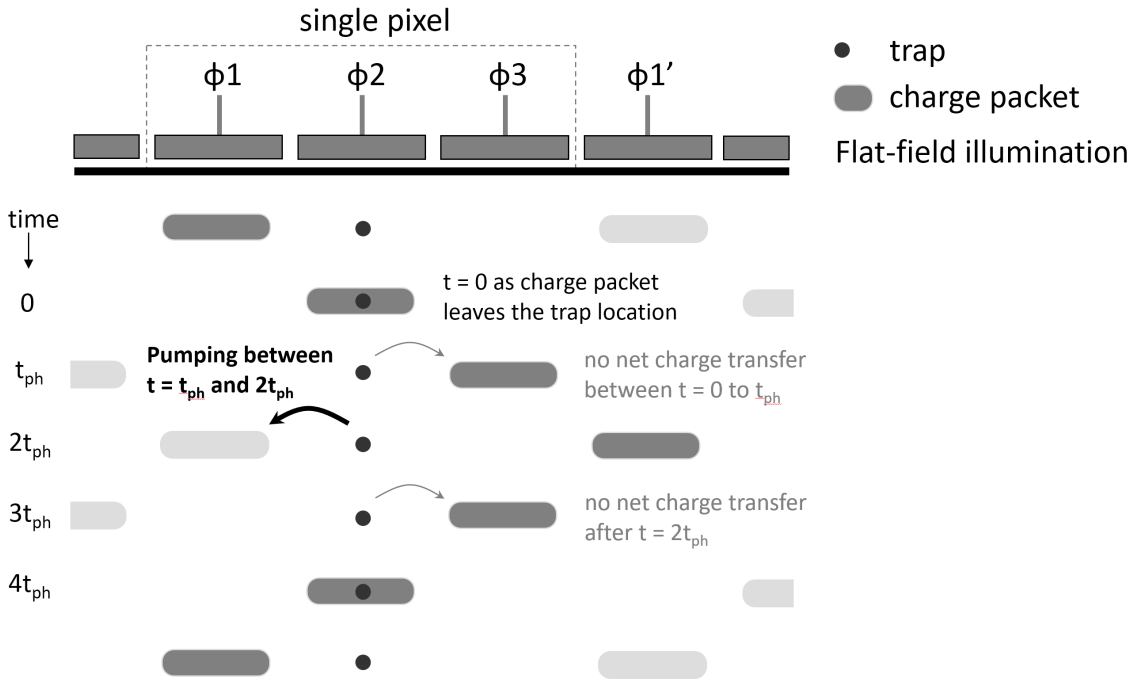

(b) Trap-pumping dynamics leading to Equation 3.1 (adapted from [8]).

Figure 2. Through the process of single-trap pumping, dipoles are formed in the image. The amplitude of the dipole will vary between different trap species, temperature and clocking frequency. It is this variation in amplitude that allows the analysis of individual traps within the CCD.

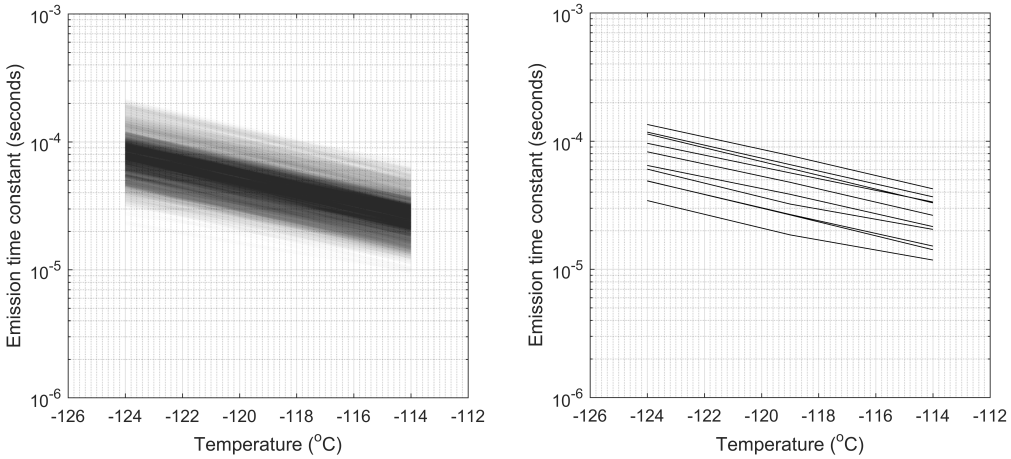

(a) The time constants for 2000 randomly selected traps, showing the "block" of trap emission time constants.

(b) The time constants for 10 randomly selected traps, showing the individual properties that are lost in the "block" shown in 3(a).

Figure 3. The time constants for two populations of traps are shown at each of the three temperatures are shown. In 3(b) we can see that the lines are relatively parallel with very small deviations from the expected curves from Shockley-Read-Hall theory. The spread is therefore thought to be genuine, with the uncertainty dominated by any deviation from the expected curve form.

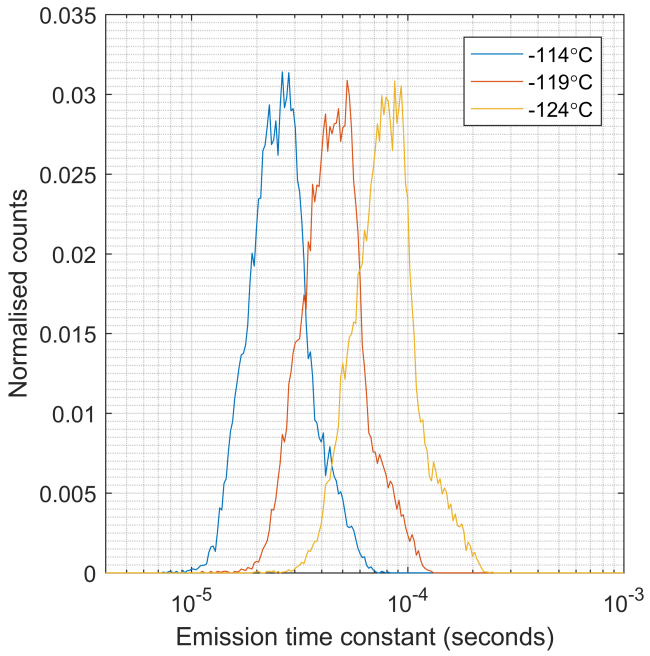

Figure 4. The distribution of time constants at the three temperatures tested. The distribution is thought to be genuine and not a measurement uncertainty, as is demonstrated in Figure 3.

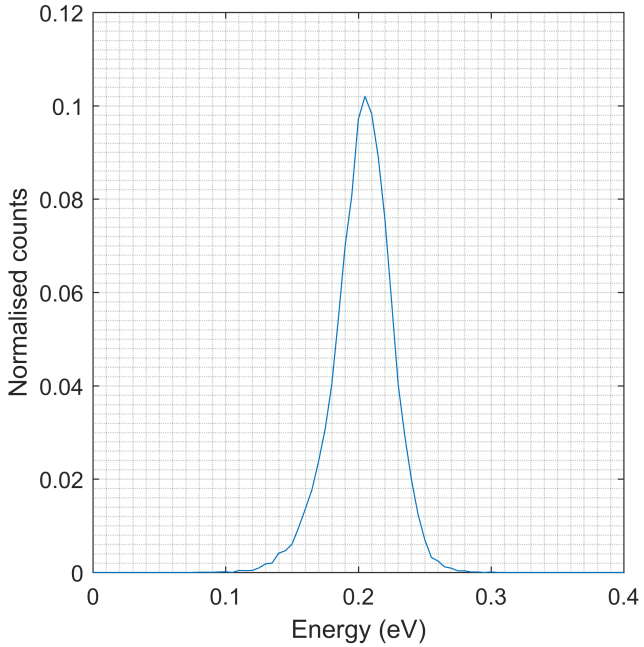

Figure 5. Through fitting the curves for each trap, examples of which are shown in Figure 3, the energy levels of the trap population above the valence band can be found. The distribution centres about 0.20 eV, with a FWHM of approximately 0.05 eV.

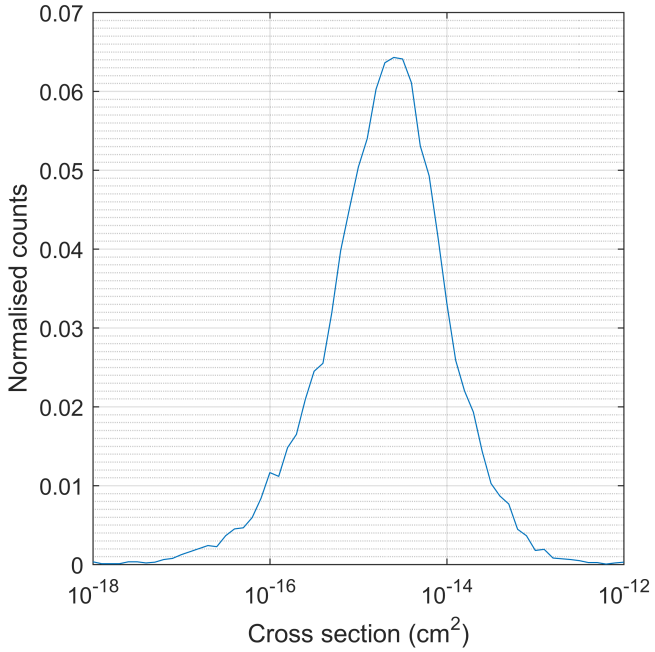

Figure 6. Through the same fitting process as that used to find the trap energy level, the cross-section can be found. The mean cross-section was found to be 3×10^{-15}.

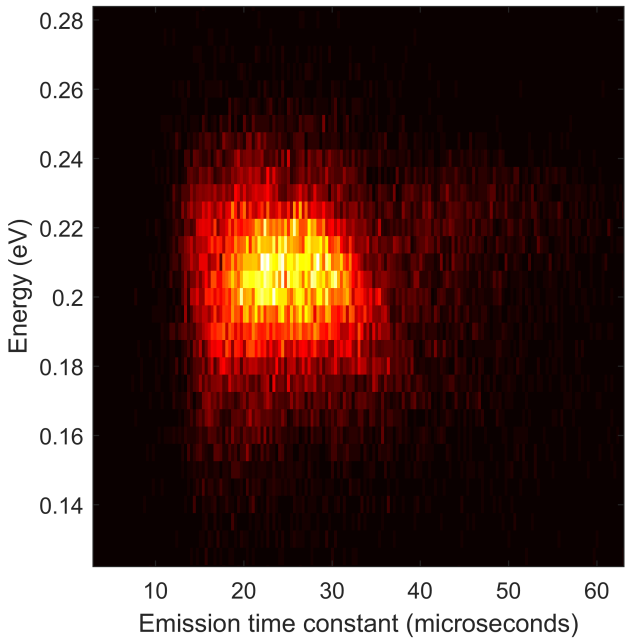

Figure 7. The emission time constants shows no correlation with energy, demonstrating a bell-shaped distribution in both time and energy.